



**HAL**  
open science

# Depth resolution enhancement of terahertz deconvolution by autoregressive spectral extrapolation

Junliang Dong, Alexandre Locquet, D. Citrin

► **To cite this version:**

Junliang Dong, Alexandre Locquet, D. Citrin. Depth resolution enhancement of terahertz deconvolution by autoregressive spectral extrapolation. *Optics Letters*, 2017, 42 (9), pp.1828. 10.1364/OL.42.001828 . hal-02347766

**HAL Id: hal-02347766**

**<https://hal.science/hal-02347766>**

Submitted on 8 Apr 2022

**HAL** is a multi-disciplinary open access archive for the deposit and dissemination of scientific research documents, whether they are published or not. The documents may come from teaching and research institutions in France or abroad, or from public or private research centers.

L'archive ouverte pluridisciplinaire **HAL**, est destinée au dépôt et à la diffusion de documents scientifiques de niveau recherche, publiés ou non, émanant des établissements d'enseignement et de recherche français ou étrangers, des laboratoires publics ou privés.

# Depth-resolution enhancement of terahertz deconvolution by autoregressive spectral extrapolation

JUNLIANG DONG<sup>1,2,\*</sup>, ALEXANDRE LOCQUET<sup>1,2</sup>, AND D. S. CITRIN<sup>1,2</sup>

<sup>1</sup>UMI 2958 Georgia Tech-CNRS, Georgia Tech Lorraine, 2 Rue Marconi, 57070 Metz, France

<sup>2</sup>School of Electrical and Computer Engineering, Georgia Institute of Technology, Atlanta, GA 30332-0250, USA

This Letter presents a method for enhancing the depth-resolution of terahertz deconvolution based on autoregressive spectral extrapolation. The terahertz frequency components with high signal-to-noise ratio are modeled with an autoregressive process, and the missing frequency components in the regions with low signal-to-noise ratio are extrapolated based on the autoregressive model. In this way, the entire terahertz frequency spectrum of the impulse response function, corresponding to the material structure, is recovered. This method, which is verified numerically and experimentally, is able to provide a 'quasi-ideal' impulse response function, and therefore, greatly enhances the depth-resolution for characterizing optically thin layers in the terahertz regime. © 2022 Optical Society of America

OCIS codes: *ciscodes*

<https://doi.org/10.1364/OL.42.001828>

Due to the penetrative capability of terahertz (THz) radiation, THz imaging has attracted considerable interest as a noninvasive, noncontact, and nonionizing modality to characterize various non-metallic multi-layered structures in industrial [1–3], biomedical [4] and cultural-heritage fields [5–7]. THz reflective imaging provides information in depth by analyzing the reflected THz signal with an incident short THz pulse. Due to dielectric discontinuities with depth, reflected temporal THz echoes associated with Fresnel coefficients between various interfaces are recorded as a function of transverse position in amplitude and time delay. The stratigraphy of multi-layered structures can be obtained based on the precise estimation of the arrival times of echoes in the reflected signal. However, when the layers of the structures are optically thin in the THz regime, the echoes may partially or totally overlap in time; therefore, when no prior knowledge of the structures is available, THz deconvolution is essential to resolve the overlapping echoes and extract the arrival times of superimposed echoes from noisy measurements.

Theoretically, the reflected THz signal  $r(t)$  is the convolution of the incident THz pulse  $i(t)$  with the impulse response function  $h(t)$ , which should ideally consist of  $M$  time-shifted ideal impulses, with the number  $M$  corresponding to the material structure; therefore, the Fourier transform of this ideal impulse response function is broadband and should be a sum of  $M$  complex sinusoids throughout the entire frequency spectrum. Conventional deconvolution based on direct inverse filtering aims at retrieving the impulse response function by applying the inverse Fourier transform of the transfer function  $H_{inv}(f)$ , which is the ratio of the reflected to the incident THz spectra,

$$h_{inv}(t) = FFT^{-1}(H_{inv}(f)) = FFT^{-1} \left[ \frac{FFT(r(t))}{FFT(i(t))} \right], \quad (1)$$

where  $FFT$  denotes the Fourier transform and  $FFT^{-1}$  the inverse Fourier transform, and  $h_{inv}(t)$  is the impulse response function obtained by directly inverse filtering. Frequently, successful deconvolution cannot be expected by directly applying Eq.1. Because the THz pulse is band-limited, with a fast-decreasing spectrum outside of the passband (in our case extending from 60 GHz to 3 THz), the division of small values due to the deficiency of THz sources in the low- and high-frequency regions, will give rise to large abnormal values as high spikes and ruin the signal-to-noise ratio there; therefore,  $H_{inv}(f)$ , as obtained from Eq.1 is only valid within the bandwidth with high SNR. Furthermore, these high spikes in the low- and high-frequency regions, where the SNR is low, will introduce severe low- and high-frequency noises in the impulse response function.

THz frequency-wavelet domain deconvolution (FWDD) [8] is specifically designed to enhance the deconvolution process by first employing frequency-domain filtering and then further improving the SNR by wavelet de-noising.

Baseline subtraction is also required to cancel the slow fluctuations corresponding to the low-frequency noise. Wiener filtering [8], double Gaussian filter [9] and van Hann filter [7, 10] can serve as the frequency-domain filtering. However, the frequency-domain filtering will narrow the bandwidth of the impulse response function by eliminating the high spikes in the low- and high-frequency regions, and only the frequency components within the bandwidth with high SNR are kept. Therefore, pulses in the impulse response function recovered by FWDD are much wider than the ideal impulses, and consequently, limit the depth-resolution.

In this Letter, we demonstrate a method for enhancing the depth-resolution of THz deconvolution based on autoregressive spectral extrapolation. This method consists in modeling part of the deconvolved spectrum with high SNR with an autoregressive (AR) process, and to extrapolate the remaining part of the spectrum based on this AR model. What underlies AR spectral extrapolation is the maximum entropy method which consists in determining a spectral estimation that maximizes uncertainty with respect to the unknown information, thus eliminating unreasonable constraints, but that is consistent with the known information [11]. Direct use of the maximum entropy method is marred, however, by the lack of criterion for determining the order of the model used. It has been shown [12] that the maximum entropy method is equivalent to the least squares fitting of an AR process for which mathematical criterion (e.g. Akaike's criterion [13]) exist to determine the length of an AR model. The existence of such a criterion is crucial to avoid over- or under-fitting. In the following, we focus on deconvolution exploiting AR spectral extrapolation, and call this method 'AR deconvolution' for convenience. Unlike FWDD, which discards the frequency components in the low-SNR regions in order to cancel the high spikes, AR deconvolution aims at finding the missing frequency components in the low-SNR regions using an AR model based on the data in the high-SNR regions. With AR deconvolution, the spectrum of the impulse response function throughout the entire frequency band can be estimated, then the inverse Fourier transform leads to a 'quasi-ideal' impulse response function can be achieved, and therefore, the resolution in depth can be enhanced.

In an AR process, each data point of  $H_i$  of a digitized signal is a weighted sum of its previous  $p$  points, plus a noise term  $N_i$ ,

$$H_i = \sum_{k=1}^p a_k H_{i-k} + N_i, \quad i > p, \quad (2)$$

where  $p$  is the order of the AR process,  $a_k$  are the AR coefficients, and  $H_i$  is known within the frequency band ( $i_L \leq i \leq i_H$ ) with high SNR. This AR model can be used as a prediction filter to find an estimate  $\hat{H}_i$  of the unknown values of  $H_i$  for  $i > i_H$  using the forward prediction equation,

$$\hat{H}_i = \sum_{k=1}^p a_k H_{i-k}, \quad i > i_H. \quad (3)$$

Similarly, we can use a backward prediction filter to find the values of  $H_i$  for  $i < i_L$ ,

$$\hat{H}_i = \sum_{k=1}^p b_k H_{i+k}, \quad i < i_L, \quad (4)$$

where  $b_k$  are the coefficients for the backward prediction filter. The optimum values for the coefficients  $a_k$  and  $b_k$  are determined by minimizing the squared error between the model and the  $N_{BW}$  ( $N_{BW} = i_H - i_L + 1$ ) available data points with high SNR.

As mentioned above, the frequency spectrum of the ideal impulse response function, of a multi-layered system, should be the superposition of a limited number of complex sinusoids, each corresponding to a layer interface. It has already been shown that [11], for a noiseless case, this kind of signal, which consists of a sum of complex sinusoids, can be modeled as an AR process with an order equal to twice the number of sinusoids; for a noisy case, this kind of signal should be modeled as an AR process with an order much higher than the number of sinusoids. Akaike's Information Criterion (AIC) [13], which is based on the principle of entropy maximization in information theory, provides a measure for the selection of the model order  $p$ , and the AIC of order  $p$  can be calculated using the residual sums of squares from regression  $S_p^2$ ,

$$(AIC)_p = N \ln(S_p^2) + 2p, \quad (5)$$

where  $N$  is the number of data points, and  $\ln$  is the natural logarithm. AIC deals with the trade-off between the goodness of fit of the model and the complexity of the model, and according to Akaike's theory, the most accurate model has the smallest AIC value. For the THz frequency spectrum, both the forward and backward prediction filters are needed to find the missing data in the low- and high-frequency regions, and the AR coefficients are obtained by minimizing the sum of the forward and backward prediction errors  $\epsilon^2$ ,

$$\epsilon^2 = \sum_{i=i_L}^{i_{PL}} |H_i - \sum_{k=1}^p b_k H_{i+k}|^2 + \sum_{i=i_{pH}}^{i_H} |H_i - \sum_{k=1}^p a_k H_{i-k}|^2, \quad (6)$$

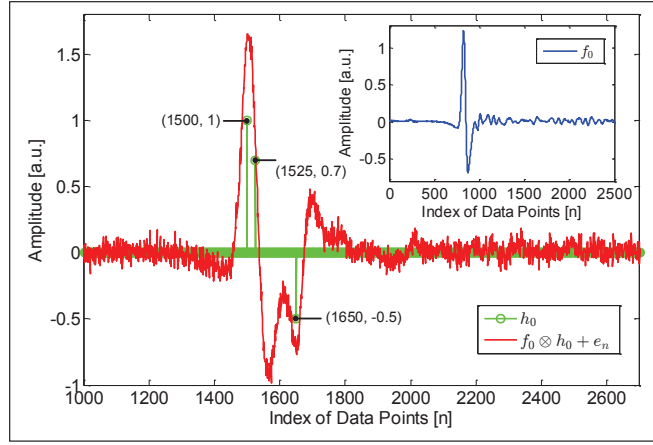


**Fig. 1.** The assumed impulse response function  $h_0$  and the simulated received THz signal  $r_0$ . The inset shows the actual THz reference signal  $f_0$ .

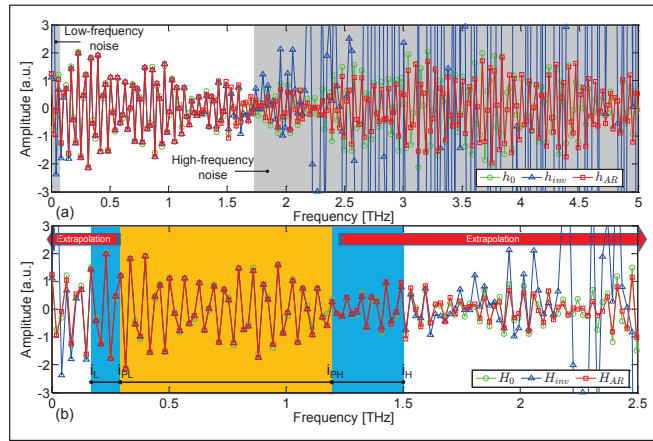


**Fig. 2.** (a) Comparison between the assumed frequency spectrum  $H_0$ , the deconvolved frequency spectrum by direct inverse filtering  $H_{inv}$  and the estimated frequency spectrum by AR spectral extrapolation  $H_{AR}$ . (b) The zoom-in of (a), which shows the detailed data allocation for the AR model.

with respect to the individual  $a_k$  and  $b_k$ . In this process, the  $N_{BW}$  available data are divided into three parts: (1) data within  $[i_{PL}, i_{PH}]$  are the  $p$  data which are kept the same and used as the base of the AR model; (2) data within  $[i_L, i_{PL}]$  are used for the fitting to find  $b_k$ ; (3) data within  $[i_{PH}, i_H]$  are used for the fitting to determine the  $a_k$ . The Burg method is utilized to minimize this error term [14]. By adding the Levinson-Durbin constraint [15], the Burg method enables the AR coefficients to be determined by a fast recursive algorithm, and guarantees a stable prediction filter, which is important to estimate the spectrum throughout the entire frequency band.

A standard THz time-domain spectroscopy (TDS) system (Teraview TPS Spectra 3000) is employed in this study to perform THz reflective imaging at almost normal incidence in order to obtain the data used in the following numerical and experimental study. The THz reference signal  $f_0[n]$ , with  $n$  as the index of data points, is recorded by setting a metal plate at the sample position, shown in the inset of Fig. 1. The data sampling period in the measurement is set to  $T_s = 0.0116$  ps. Each recorded reflected temporal THz waveform contains 4096 data points, and the signal is averaged over 10 shots. With this setting, the entire frequency spectrum obtained by Fourier transform is from 0 THz to 85.99 THz, which also contains 4096 data points.

Numerical simulations are first performed to verify the AR deconvolution. An ideal impulse response function  $h_0[n]$ , which contains 4096 data points with the same sampling period  $T_s$ , is assumed and shown in Fig. 1.  $h_0[n]$  represents a simple two-layered structure, and the time interval between the peaks are  $25T_s$  and  $125T_s$ , corresponding to the thickness of each layer.  $h_0[n]$  is convolved with the reference signal  $f_0[n]$  to simulate the received signal  $r_0[n]$ .  $e[n]$  represents the additive white noise, with which the SNR of  $r_0$  is set to be 10 dB in this simulation.

The assumed frequency spectrum  $H_0$ , which ideally consists of a sum of three complex sinusoids and is not bandlimited throughout the frequency band (from 0 THz to 85.99 THz), is obtained by the Fourier transform of  $h_0$ . In Fig. 2(a),  $H_0$

is compared with  $H_{inv}$ , which is the direct division of the spectra of  $r_0$  and  $f_0$ . By comparison, the low-SNR frequency bands of  $H_{inv}$  which contain high spikes corresponding to low- and high-frequency noises, and the high-SNR frequency band can be well separated and clearly identified. The THz frequency spectrum has a large bandwidth with high SNR, which enables us to establish an AR model with a high order. Considering the THz bandwidth and the SNR of our TDS system, we fit the AR model to the  $N_{BW}$  available data with  $i_L = 0.17$  THz and  $i_H = 1.5$  THz. By setting  $i_{PL} = 0.3$  THz and  $i_{PH} = 1.2$  THz, we allocate the data within  $[0.3, 1.5]$  for the forward prediction filter, and the data within  $[0.17, 1.2]$  for the backward prediction filter.  $AIC$  values with different orders are calculated and shown in the inset of Fig. 3. The smallest  $AIC$  value is achieved when  $p$  equals to 44. Fig. 2(b) shows the detailed data allocation for this AR process. After fitting this AR model to the  $N_{BW}$  available data, we apply this AR model as a prediction filter to extrapolate the data to find the missing data in the regions below 0.18 THz and above 1.5 THz (up to 85.99 THz). Note that this is well outside the bandwidth of our imaging system; the ability to recover data out to this high frequency depends on our having sufficient knowledge of the frequency spectrum to construct an accurate AR model. The estimated frequency spectrum  $H_{AR}$  based on this AR model is shown in red in Fig. 2. By comparison between  $H_{AR}$  and  $H_0$ , we can find out that the estimated frequency components in  $H_{AR}$  match the assumed data in  $H_0$  quite well, which verifies the effectiveness of this AR model to recover the missing data. By simply performing the inverse Fourier transform of  $H_{AR}$ , the deconvolved signal  $h_{AR}$ , can be achieved.

In Fig. 3,  $h_{AR}$  is compared with  $h_{FWDD}$ , which is the deconvolved signal obtained by FWDD, and the assumed impulse response function  $h_0$ . For FWDD, van Hann filter is selected to serve as the frequency-domain filter to suppress the high-frequency noise, and the maximum value of the cutoff frequency we can set is  $f_c = 3.5$  THz in order to obtain a satisfactory SNR of the deconvolved signal. More details about the FWDD algorithm we use can be found in [16]. With FWDD, only the first and the third interface can be identified, and the first assumed layer with time interval  $25T_s$  (corresponding to an air gap with thickness of  $43.5 \mu m$ ) cannot be resolved. In contrary,  $h_{AR}$  is able to resolve all the interfaces, and exhibits a 'quasi-ideal' impulse response function compared with the assumed impulse response function  $h_0$ . Based on this simulation, we can conclude that the minimum thickness resolved by THz reflective imaging, is enhanced by AR deconvolution, since the frequency components throughout the entire spectrum are estimated and recovered. It is important to note that the minimum thickness (time interval) resolution, corresponding to the depth-resolution, is mainly dependent on the bandwidth of the THz source, the sampling frequency and the SNR. In our simulations, the minimum time interval which can be resolved by AR deconvolution with the SNR = 10 dB is  $15T_s$  (corresponding to an air gap with thickness of  $26.1 \mu m$ ); on the other hand, the minimum time interval resolved by FWDD with the same SNR is  $30T_s$ . Therefore, the depth-resolution can be increased by a factor of two using AR deconvolution.

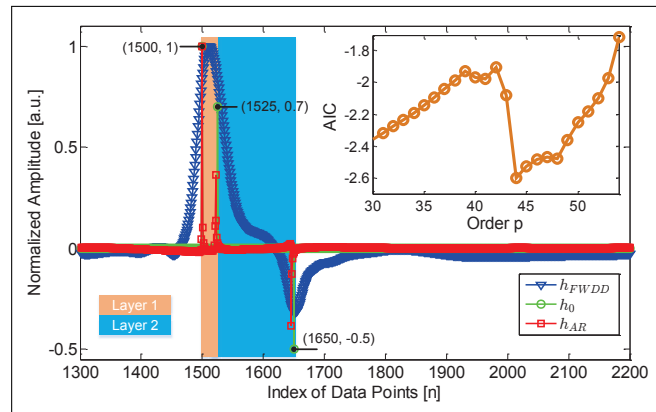


**Fig. 3.** Comparison of the simulated deconvolution results obtained by AR deconvolution with  $p = 44$ , FWDD and the assumed impulse response function. The inset shows the  $AIC$  values with different model orders.

Next, a one-layered polymer coating on a steel substrate is employed in this study to verify the effectiveness of AR deconvolution experimentally. The thickness of the polymer coating is about  $22.5 \mu m$ , which is thin in the THz regime. THz reflective imaging experiment was performed, and the typical waveform received is shown in the inset of Fig. 4(a). Since the coating is very thin and the steel substrate provides total reflection, the reflected signal is similar to the reference signal and no overlapping echoes can be observed in time domain. Both FWDD and AR deconvolution are performed to resolve this thin coating layer. In the deconvolution, we consider the THz reference signal as the input and the received THz signal as the output; therefore, the actual impulse response function associated with the Fresnel coefficients can be obtained by multiplying the deconvolved signal by a factor of  $-1$  for phase correction. For FWDD, the maximum cutoff frequency leading to a satisfactory SNR in time domain is 4 THz; For AR deconvolution, we set the parameters the same as the ones we used in the simulation. Based on the AR model, the frequency components outside the frequency

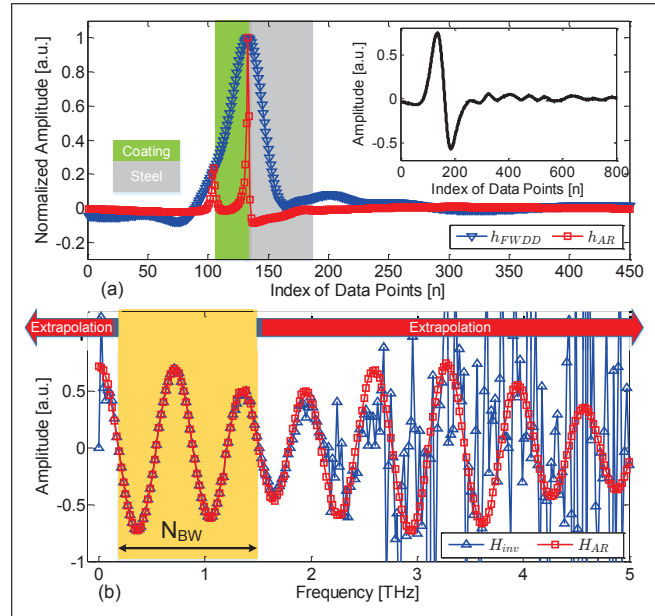


**Fig. 4.** (a) The deconvolution results based on FWDD and AR deconvolution. The inset shows the received THz signal reflected from the poly-coated steel sample; (b) The estimated frequency spectrum (up to 5 THz) based on autoregressive spectral extrapolation.

window with high SNR are estimated and the entire frequency spectrum of the impulse response function is recovered successfully. The frequency spectrum should ideally consist of two sinusoids, shown in Fig. 4(b). The deconvolution results based on FWDD and AR deconvolution are shown in Fig. 4(a). Compared with the deconvolved result by FWDD, which only shows one peak, the deconvolved signal based on AR deconvolution successfully resolves the thin coating layer and presents a clear representation of the sample structure. Therefore, we can conclude that the resolution in depth can be significantly enhanced by AR deconvolution.

In this Letter, AR deconvolution which is based on autoregressive spectral extrapolation, is presented to enhance the depth-resolution of THz deconvolution. The de-noising procedure in the conventional deconvolution, such as FWDD, narrows the bandwidth of the impulse response function by eliminating the frequency components in the low-SNR regions, and therefore, lowers the resolution in-depth. On the contrary, AR deconvolution aims at recovering the missing frequency components in the low-SNR regions using the AR model based on the frequency components in the high-SNR regions. In this way, the entire spectrum of the impulse response function is estimated, and a 'quasi-ideal' impulse response function with enhanced depth-resolution is achieved. We find out AR deconvolution is very suitable to deal with THz TDS signals, as the THz spectrum provides a large bandwidth with high SNR to establish a high-order AR model. It is also important to note that the deconvolution result is sensitive to the selection of parameters and SNR when a high-order AR model is utilized. This method is verified numerically and experimentally with a one-layered polymer coating with thickness of  $22.5 \mu\text{m}$ , which cannot be resolved by FWDD. The thickness is successfully resolved by AR deconvolution, demonstrating that AR deconvolution enables us to beat the limitation of the THz wavelength and enhance the depth-resolution for resolving the optically thin layers in the THz regime.

The authors gratefully acknowledge the financial support of the Conseil Régional du Grand Est of the Fonds Européen de Développement Régional (FEDER), and of the Institut Carnot ARTS.

## REFERENCES

1. K. Su, Y. C. Shen, and J. A. Zeitler, "Terahertz sensor for non-contact thickness and quality measurement of automobile paints of varying complexity", *IEEE Trans Terahertz Sci. Technol.* **4**, 432-439 (2014).
2. J. Dong, B. Kim, A. Locquet, P. McKeon, N. Declercq, and D. S. Citrin, "Nondestructive evaluation of forced delamination in glass fiber-reinforced composites by terahertz and ultrasonic waves", *Compos. Part B. Eng.* **79**, 667-675 (2015).
3. H. Lin, Y. Dong, Y. C. Shen, and J. A. Zeitler, "Quantifying pharmaceutical film coating with optical coherence tomography and terahertz pulsed imaging: an evaluation", *J. Pharm. Sci.* **104**, 3377-3385 (2016).
4. E. P. J. Parrot, S. M. Y. Sy, T. Blu, V. P. Wallace, and E. Pickwell-MacPherson, "Terahertz pulsed imaging in vivo: measurements and processing methods", *J. Biomed. Opt.* **16**, 106010-106010 (2011).
5. M. Schwerdtfeger, E. Castro-Camus, K. Krügener, W. Viöl, and M. Koch, "Beating the wavelength limit: three-dimensional imaging of buried subwavelength fractures in sculpture and construction materials by terahertz time-domain reflection spectroscopy", *Appl. Opt.* **52**, 375-380 (2013).
6. C. L. Koch-Dandolo, T. Filtenborg, K. Fukunaga, J. Skou-Hansen, and P. U. Jepsen, "Reflection terahertz time-domain imaging for analysis of an 18th century neoclassical easel painting", *Appl. Opt.* **54**, 5123-5129 (2015).
7. J. Dong, J. Bianca Jackson, M. Melis, D. Giovanacci, G. C. Walker, A. Locquet, J. W. Bowen, and D. S. Citrin, "Terahertz frequency-wavelet domain deconvolution for stratigraphic and subsurface investigation of art painting", *Opt. Express* **24**, 26972-26985 (2016).
8. Y. Chen, S. Huang, and E. Pickwell-MacPherson, "Frequency-wavelet domain deconvolution for terahertz reflection imaging and spectroscopy", *Opt. Express* **18**, 1177-1190 (2010).
9. Y. Chen, Y. Sun, and E. Pickwell-MacPherson, "Total variation deconvolution for terahertz pulsed imaging", *Inverse Probl. Sci. Eng.* **19**, 223-232 (2011).
10. R. K. H. Galvão, S. Hadjiloucas, A. Zafiroopoulos, G. C. Walker, J. W. Bowen, and R. Dudley, "Optimization of apodization functions in terahertz transient spectrometry", *Opt. Lett.* **32**, 3008-3010 (2007).
11. T. J. Ulrych, R. W. Clayton, "Time series modelling and maximum entropy", *Phys. Earth Planet In.* **12**, 188-200 (1976).
12. T. J. Ulrych, T. N. Bishop, "Maximum entropy spectral analysis and autoregressive decomposition", *Rev. Geophys.* **12**, 183-200 (1975).
13. H. Akaike, "A new look at the statistical model identification", *IEEE Trans. Automat. Control* **19**, 716-723 (1974).
14. B. Shakibi, F. Honarvar, M. D. C. Moles, J. Caldwell, and A. N. Sinclair, "Resolution enhancement of ultrasonic defect signals for crack sizing", *NDT E Int.* **52**, 37-50 (2012).
15. M. Ortigueira, and J. Tribolet, "Global versus local minimization in least-squares AR spectral estimation", *Signal Processing* **7**, 267-281 (1984).
16. J. Dong, A. Locquet, and D. S. Citrin, "Terahertz quantitative nondestructive evaluation of failure modes in polymer-coated steel", *IEEE J. Sel. Top. Quantum Electron.* **23**, 1-7 (2017).